Multimodal gadolinium oxysulfide nanoparticles for bioimaging: A comprehensive biodistribution, elimination and toxicological study

Julien Santelli, Séverine Lechevallier, Denis Calise, Dimitri Marsal, Aurore Siegfried, Marine Vincent, Cyril Martinez, Daniel Cussac, Robert Mauricot, Marc Verelst

Version of Record: https://www.sciencedirect.com/science/article/pii/S1742706120301458
Manuscript_e8d0cd797906ea27b784913c79be20d5

Multimodal Gadolinium Oxysulfide Nanoparticles for Bioimaging: A Comprehensive Biodistribution, Elimination and Toxicological study.

Julien Santelli[(a, b)],SéverineLechevallier[(c)],Denis Calise[(b)], Dimitri Marsal[(b)], Aurore Siegfried[(b)],Marine Vincent[(b)],Cyril Martinez[(c)], Daniel Cussac[(b)], Robert Mauricot [(a)] and Marc Verelst[(a,c)*]

a) CEMES-CNRS, Université de Toulouse, CNRS, 29 rue Jeanne Marvig BP 94347, 31055 Toulouse cedex 4, France

b) I2MC, Université de Toulouse, INSERM, Hôpitaux de Toulouse, France

c) CHROMALYS SAS, 29 rue Jeanne Marvig, 31400Toulouse, France

Abstract

For some years now, gadolinium oxysulfide nanoparticles (NPs) appear as strong candidates for very efficient multimodal *in vivo* imaging by: 1) Magnetic Resonance (MRI), 2) X-ray Computed Tomography (CT) and 3) photoluminescence imaging. In this paper, we present a selection of results centered on the evaluation of physico-chemical stability, toxicity, bio-distribution and excretion mechanisms of $Gd_2O_2S:Ln^{3+}$ nanoparticles intravenously injected in rats. Two formulations are here tested with a common matrix and different dopants: $Gd_2O_2S:Eu^{3+}{}_{5\%}$ and $Gd_2O_2S:Yb^{3+}{}_{4\%}/Tm^{3+}{}_{0.1\%}$. The NPs appear to be almost insoluble in pure water and human plasma but corrosion/degradation phenomenon appears in acidic conditions classically encountered in cell lysosomes. Whole body *in vivo* distribution, excretion and toxicity evaluation revealed a high tolerance of nanoparticles with a long-lasting imaging signal associated with a slow hepatobiliary clearance and very weak urinary excretion. The results show that the majority of the injected product (> 60%) has been excreted through the feces after five months. Experiments have evidenced that the NPs mainly accumulate in macrophage-rich organs, that is mainly liver and spleen and to a lesser extent lungs and bones (mainly marrow). No significant amounts have been detected in other organs such as heart, kidneys, brain, intestine and skin. $Gd_2O_2S:Ln^{3+}$ NPs appeared to be very well tolerated up to 400 mg/kg when administered intravenously.

Keywords: Nanoparticles; Lanthanides; Biodistribution; Toxicity; Bioimaging; Multimodality

Introduction

Lanthanides (Ln) are the 15 elements, ranging from lanthanum to lutetium in the periodic table. Lanthanide-based NPs have now been long considered for bioimaging [1] because Ln^{3+} ions, show advantageous optical characteristics including excellent photostability, large Stokes/anti-Stokes shifts, long luminescent lifetimes, and sharp-band emissions. Ln^{3+}-doped upconversion nanoparticles (UCNPs) are now intensively studied for biological applications [2] because the Near InfraRed (NIR) excitation allows for deeper penetration into biological tissues than traditional fluorescent probes. In addition, they are completely insensitive to the photo-bleaching phenomenon which allows the use of very high excitation powers only limited by biological tissues heating. Therefore, Ln^{3+} UNCP are promising luminescent nanoprobes for bioimaging applications [3].

Additionally, unpaired 4f electrons of lanthanides (up to seven for Gd^{3+}) possess strong unquenched angular momentum, leading to an effective spin–orbit coupling and interesting paramagnetic properties (except La^{3+} and Lu^{3+}). More particularly, Gd^{3+} ion possess a weak spin–orbit coupling and consequently a long electronic relaxation time. Therefore, Gd^{3+} complexes have been intensively studied and are now used as contrast agents (CAs) in magnetic resonance imaging (MRI) because they strongly reduce relaxation time of protons and greatly enhance image contrast [4].

Because Ln^{3+} NPs may contain a very high payload of paramagnetic ions, they have been recently developed for MRI [5]. Ln^{3+} NPs (especially Gd-based) with well controlled size and crystallinity should then offer great opportunities for CAs [6–8] and could constitute an interesting alternative to the Gd^{3+} complexes which often have a relatively poor stability.

To date, a wide panel of inorganic matrixes have been investigated for doping Gd^{3+}ions [1]. Among all candidates, Gd_2O_3 became the prototype of Gd-based inorganic NPs used as CAs, and relevant studies were expanding [1]. GdF_3 and $NaGdF_4$ have also been widely studied as MRI CAs [9–13]. Finally, Gd being a heavy element, it presents fair contrast properties in X-ray Computed Tomography (CT) [12,14].

It is in this context that we have proposed in 2011 [15] then 2014 [16] to focus on gadolinium oxysulfide nanoparticles for multimodal imaging using fluorescence, MRI and CT. This work has then been completed by other studies [17–21] which have also demonstrated the interest of this gadolinium oxysulfide matrix for bio-imaging. Indeed, this oxysulfide matrix has very interesting properties compared to oxide or fluoride NPs which have been much more extensively studied: i) the presence of sulphide S^{2-}ion in the structure introduces a very efficient 340 nm centered charge transfer absorption band which can be very advantageously used on any fluorescence microscope (or flow cytometer) conventionally equipped with a 360 nm laser (often used for DAPI dye excitation). Such a possibility of easy excitation in the near UV does not exist in oxides or fluorides [15]. ii) the Gd oxysulfide matrix

also shows excellent properties in NIR imaging using upconversion phenomenon which is much better than for the oxides [16]. Data is still scarce to compare with $NaGdF_4$ based matrix, but according to our preliminary experiment, performances are comparable. This has been established in the recent years for Gd_2O_2S:Yb/Er UCNPS [16,17,22,23] (λ_{exc}=980nm, λ_{em}=670nm). However, we have very recently determined that Gd_2O_2S:Yb/Tm UCNPS [21] seem to be even more efficient. They present a very intense emission peak centered on 802 nm, exactly corresponding to the biological tissues minimum absorption [24]. iii) if very small nanoparticles (<10nm) of gadolinium oxides or fluorides show very good contrast properties in T_1 MRI, larger Gd oxysulfide particles (≈100nm) show very good properties in T_2 imaging [16] and are therefore an interesting complementary product. iv) Gd_2O_2S matrix is at the basis of the best scintillator materials (visible light emission under X-ray excitation) known today [15], leaving the possibility to use XEOL (X-Ray Excited Optical Luminescence) or XLCT (X-Ray Luminescence Computed Tomography) whose proof of concept has already been demonstrated since 2010 [25–28]. Finally, v) it has been demonstrated very recently that the Gd_2O_2S:Yb/Er matrix shows interesting properties in thermometry [29], which opens up a new type of potential application in biology and medicine.

However, since the European Medicines Agency (EMA) has recommended to restrict the use of some linear gadolinium agents used in MRI [30], a particular attention must be paid to any new contrast media containing gadolinium. The problem stems from the instability of the first-generation of linear complexes that tend to release (or exchange) potentially toxic ionic Gd^{3+} that can cause nephrogenic fibrosis [31] and accumulate in the brain [32]. From the point of view of a material scientist, it is quite clear that in Ln^{3+} mineral NPs, the dissociation and consequent Gd^{3+} leakage are minimized because they are entrapped in a rigid and insoluble crystal structure [33]. Nonetheless, it is indispensable to characterize the *in vivo* behavior of these new kind of nano-markers to assess their potential toxicity, if one wants to consider a more global use in preclinical (and eventually clinical) studies. This is the main purpose of this work.

Some recent results obtained on cell cultures have already revealed the very low toxicity of Gd_2O_2S:Ln^{3+} NPs [15,16,18–20,27] but very few and partial results have yet been presented *in vivo* [19,20]. This field remains to be documented more widely; therefore, we here present a compilation of studies evaluating toxicity, bio-distribution and excretion mechanisms of intravenously injected Gd_2O_2S:Ln^{3+} nanoparticles. This work focuses on the *in vivo* behavior of two Gd_2O_2S:Ln^{3+} NPs compositions: Gd_2O_2S:$Eu^{3+}{}_{5\%}$ and Gd_2O_2S:$Yb^{3+}{}_{4\%}$/$Tm^{3+}{}_{0.1\%}$ (used for NIR imaging) as well as their *in vitro* chemical and biological stability in aqueous media.

Materials and methods

General Chemicals

Gadolinium and ytterbium (99.9%) were purchased from Strem. Europium and thulium nitrates (99,99%) were stock solutions from Rhodia. Urea (98) ethanol (99%), sulfur, polyethylene glycol (Mw=3000), ultrapure distilled nitric acid (HNO_3, 70%), hydrogen peroxide (H_2O_2, 30%) and glucose were purchased from Sigma Aldrich. CD3 and CD20 antibodies were purchased from Roche (2GV6) and Invitrogen (L26).

Synthesis of the precursors

Gadolinium hydroxycarbonates were synthesized as previously described [15,16]. Briefly, lanthanide nitrates and urea were dissolved in a solution of water and ethanol (80/20vol%). The optimum concentrations used in this work were $[Ln]_{Total}=5.6x10^{-3}$ M and [urea]=0.5 M. For Eu and Yb/Tm doping, the molar compositions used were [Eu]/([Gd]+[Eu]) = $5\%_{mol}$ and [Tm]/([Gd]+[Yb]+[Tm]) = $0.1\%_{mol}$, [Yb]/([Gd]+[Yb]+[Tm]) = $4\%_{mol}$. The solution was placed in beaker for aging at 85°C, during 100 min under agitation. The suspension was then centrifuged for 2 hours at 4000g. The supernatant solution was discarded, and the solid phase was resuspended in water 3 times. The solid phase was then dried in an oven at 85 °C overnight.

$Gd_2O_2S:Ln^{3+}$ NPs synthesis

Gadolinium oxysulfide NPs were synthesized following two steps [15,16]. First, the hydroxycarbonates were oxidized at 750 °C for 4 h. Second, the oxides underwent a solid-gas sulfuration by annealing at 850 °C for 4 h in the presence of sulfur under an inert gas flow of argon. After cooling to room temperature, $Gd_2O_2S:Ln^{3+}$ NPs were obtained and characterized.

$Gd_2O_2S:Ln^{3+}$ injection solution preparation

500 mg of $Gd_2O_2S:Ln^{3+}$ NPs were dispersed in 50 mL of ultrapure water (Milli-Q) and stabilized by 5 equivalents of polyethylene glycol (PEG; Mw=3000). The suspension was then stirred at 50°C for 24h to allow for PEG adsorption on the surface of the NPs. Then, the nanoparticle suspension was slowly centrifuged (600g, 5 minutes) in order to remove unwanted aggregates (which may cause embolization problems during IV injection). Only the supernatant was preserved and analyzed to determine its concentration. It was then diluted with a glucose solution in order to reach the targeted NPs concentration and isotonicity (final glucose concentration: 5%). The solution was stored at 4°C for a maximum duration of one week. Just before injection, it was re-dispersed by sonication using an ultrasonic wave bath.

Physico-chemical characterization

XRD patterns were collected using a Brucker D8 Advance diffractometer attached with a linear detector and a Cu-Kα source operating at 40 mA and 40kV. The scan range was set from 10 to 80 °2θ with a step size of 0.02 ° and a count time of 13s. The shape and size of the nanoparticles were examined with a transmission electron microscope (TEM; Philips CM20 FEG). The luminescence of solid samples was studied with a Jobin-Yvon Model Fluorolog FL3-22 spectrometer that was equipped with a R928 Hammamatsu photomultiplier and a 450 W Xe excitation lamp or an externally conducted 980 nm fiber laser as excitation source. All emission spectroscopy were performed at room temperature.

***In vitro* degradation study**

$Gd_2O_2S:Eu^{3+}_{5\%}$ NPs were suspended at a concentration of 10 mg/mL in ultrapure water (Milli-Q), human plasma (Seralab) or buffered lysosomal simulated environment [34] (100 mL of PBS, 647 mg of citrate sodium, $HCl_{3.7\%}$to reach a pH=4.5). The solutions were then sonicated for 30 min to ensure a good particle dispersion and aliquoted in 2 mL aliquots. Each aliquot were kept at 37°C for aging. At each time point, an aliquot was centrifuged (10000g, 30 min) to separate the NPs from the supernatant containing soluble Gd^{3+} species (and no NPs). The concentration was then determined by ICP-OES (Horiba, Ultima 2).

Experimental animals

Animal experimentations were conducted in accordance with the European Communities Council Directive (2010/63/UE) for experimental animal care and were approved by local animal care and use committees C2EA – 18 and C2EA – 122 (Comités D'éthique En Expérimentation Animale) controlled by the C.N.R.E.E.A (Comité National de Réflexion Éthique sur l'Expérimentation Animale, French Ministry of Higher Education, of Research and Innovation) and registered under the project accreditation numbers 3899 and 7641. 7 weeks old female Lewis and Wistar rats (Janvier Labs) were housed in an air-conditioned room with 12 h light and dark cycles in a controlled environment at a temperature of22 ± 2 °C and a relative humidity of 45%. The animals occupied standard cages with free access to food and water *ad libitum*.

Assessment of biodistribution, excretion and potential side-effects of PEG-$Gd_2O_2S:Ln^{3+}$ NPs

Intravenous injection in rats

Before injection, animals were anesthetized in a chamber using 3% isoflurane in O_2 and maintained at 1-2% isoflurane through a mask afterwards. An injection of 0.33 mL/Kg of buprenorphine (Buprecare,

0.3 mg/mL) was administered before any surgical operation. A single intravenous (IV) injection of the PEG-$Gd_2O_2S:Ln^{3+}$ NPs solution was performed in each experiment.

PEG-$Gd_2O_2S:Yb^{3+}_{4\%}/Tm^{3+}_{0.1\%}$ NPs (0.862 mg/mL, 4 mL/kg) were injected in the jugular vein of 6 Lewis rats using a 32 G cannula and a PE10 catheter connected to a syringe pump. Injection rate was maintained at 5 mL/h and NIR detection was performed simultaneously. Hence, 3.45 mg/kg of NPs were injected, corresponding to 560 µg of NPs (or 464 µg of gadolinium) when reported to the body weights. This quantity is about 5 times less than what is usually used in MRI scans (0.1 mmol/Kg or 15.7 mg/Kg of Gd) with commercial Gd-based contrast agents like Dotarem® [35].

PEG-$Gd_2O_2S:Eu^{3+}_{5\%}$ NPs (3.35mg/mL, 4 mL/Kg) were injected in the caudal vein of 6 Wistar rats using a 24G needle. The solutions were injected slowly (5 to 7 min) to avoid embolism. Hence, 13.3mg/kg of NPs were injected; which corresponds to a total quantity of 3337 µg of NPs (or 2776 µg of gadolinium).

Control animals (6 Lewis rats and 1 Wistar rat) received an injection of isotonic 5% glucose solution.

Measurements and monitoring were then followed depending on the injected NPs. The measurement timeline as well as the injection protocol are synthesized in Fig.S1 (supplementary material). The clinical status and body weight have been tracked throughout the studies to check for potential side effects on animal's health.

NIR live imaging

The biodistribution of PEG-$Gd_2O_2S:Yb^{3+}_{4\%}/Tm^{3+}_{0.1\%}$ NPs was monitored over-time using a NIR custom-made imaging system already described in a previous paper [21]. The system consists of: a 980 nm laser diode (MDL-N-980/6000~1000mW) coupled with an optical fiber, a laser clean-up filter (LD01-975/10, Semrock) and a beam expander (BE05M-B, Thorlabs) allowing a ⌀ 2.8 cm circular illumination area for excitation. For acquisition, a CCD camera (iKon-M 934, Andor) equipped with a 35 mm focal length lens (LM35XC, Kowa), two bandpass filters (FF01-842/SP25, Semrock), one shortpass blocking edge filter (FF01-890/SP25, Semrock), a dichroic filter (DMSP950R, Thorlabs) were used. These filters were placed in front of the camera lens to cut the reflected excitation light, and let pass all visible luminescence emissions. The optical power was measured with a power meter (PM130D, Thorlabs). All images were obtained with an excitation laser beam power density of 110mW/cm^2 and were collected at room temperature.

Every imaging session was performed under general anesthesia (1-2% isoflurane with gas mask) and hair removal was performed before laser illumination to minimize the diffusion along the hairs that could lead to tissue damage.

Every image was acquired using the Andor Solis camera software as a set of two complementary pictures: one NIR picture during laser illumination and one white light image. Image processing was performed with the FIJI software [36]: the sets of images were merged with a dedicated lookup table for false coloring of the fluorescence signal. As the laser illumination area is not large enough to cover the whole animal, different acquisitions were performed on strategical anatomical locations and full body reconstruction of the different images was achieved using the Mosaic J plugin [37]. The signal/noise ratio was determined dividing the mean value of the region of interest by the mean value of the surrounding background.

Biological sampling

Biological samples were regularly collected throughout the study. Blood (at least 500 µL per animal) was drawn from the caudal vein under gas anesthesia using 26 G needles and heparinized syringes and then deposited into Heparin/Lithium tubes. Urine (at least 1 mL) and feces (at least 200 mg) were collected by placing the animals in individual metabolism cages for 9 h (overnight). Once collected, the samples were stored at -20 ± 5°C until mass spectrometry analysis.

At experiment end points, animals were euthanized under gas anesthesia by lethal injection of 150 mg/Kg of pentobarbital (Ceva santé animale, 54.7 mg/mL). The main organs (brain, heart, lungs, liver, spleen and kidneys) were then systematically collected on each animal. Skin (from ears, back and thorax), bowel (small intestine) and bones (femurs, humerus and thoracic vertebrae T11 and attached ribs) were collected on some animals to determine potential subsidiary NPs fixation. The marrow was isolated by flushing with PBS using a 26G needle after sectioning the epiphysis. After centrifugation, the supernatant, the pelleted marrow and the mineral part (diaphysis) of the bone were analyzed separately.

The organs were then fixed in 1% PFA at 4°C over 48 h. After fixation, each organ was divided and prepared for mass spectrometry and/or histological analysis.

Mass spectrometry analysis

Before analysis, the different samples were prepared as follows:

Feces and organs were dissolved in a mixture composed of HNO_3 (1mL) and H_2O_2 (0.2 mL) in a closed and hermetic Teflon beaker heated at 135°C during 24h. The solution was then diluted in 10 mL or more in HNO_3 according to the estimated calculated concentrations.

Blood and urine (200 µL of the sample) were diluted in 3.8 mL of a mixture composed of HNO_3 0.05 N,0.05% Triton X100 and 1% ethanol).

Gadolinium concentration (reflection of the NPs) was then determined with an Inductively Coupled Plasma Mass Spectrometry (ICP-MS) iCAP TQ (ThermoScientific) device, with an indium internal

standard (at 2 µg/L).A Gd calibration curve (0 to 10 µg/L) has been realized with internal standard addition.

Histological analysis

After PFA fixation, the organs were included in paraffin and histological slices were either stained with haemalun–eosin or sirius red or incubated with anti CD3 and anti CD20 antibodies with a Benchmark XT instrument (Roche) to detect T and B cells. Thorough examination of the slices was performed to compare the control and nanoparticle-injected animals on: general anatomy, necrosis, fibrosis and immune cell infiltration.

Statistical analysis

Results in Figure 2 are presented as mean with error bars corresponding to experimental/measurement variations (estimated at 8%). Results in every other figure are expressed as mean ± SEM corresponding to biological sample variability (at least three different experiments or animals). The Area Under Curve (AUC) was calculated using GraphPad Prism.

Results and discussion

NPs characterization

Physico-chemical characterization of the $Gd_2O_2S:Ln^{3+}$ NPs after synthesis has now been well established by previous studies [15,16,20,21]. Electron microscopy images show that the $Gd_2O_2S:Ln^{3+}$ particles have a spherical shape (Fig.1A) with a narrow size distribution centered on 130 nm (± 10-15%, see Fig.S2). Those dimensions present the advantages of being easily reproducible with good imaging efficiency. XRD patterns (Fig.1B) of the final products exhibit well developed peaks, characteristic of gadolinium oxysulfide, all peaks can be indexed on the hexagonal phase of the Gd_2O_2S (ICDD File card no 020-1422). No extra peaks coming from any impurity were detected. Characterization of the multimodal imaging potential of both $Gd_2O_2S:Eu^{3+}{}_{5\%}$ and $Gd_2O_2S:Yb^{3+}{}_{4\%}/Tm^{3+}{}_{0.1\%}$ NPs was previously achieved by us [15,16,20,21]. As stated above, the common Gd_2O_2S matrix is a very good contrast agent for X-ray tomography/radiography and T_2 MRI [16]. The addition of dopants within this matrix brings luminescence properties. When excited at 365 nm, the $Gd_2O_2S:Eu^{3+}{}_{5\%}$ NPs display a predominant luminescence centered at 624 nm and other less intense peaks centered at 580, 593 and 703 nm (Fig.1C). These optical properties are particularly useful for epifluorescence microscopy as already described elsewhere [15,16,20]. When excited with NIR 980 nm wavelength, the $Gd_2O_2S:Yb^{3+}{}_{4\%}/Tm^{3+}{}_{0.1\%}$ NPs display a predominant NIR luminescence centered at 802 nm and other less intense red and blue contributions centered at 700, 650 and 480 nm (Fig.1D). These optical

properties are particularly useful for fluorescent bioimaging on live animals as already described in another paper [21] as they take advantage of the biological tissues transparency window [24,38].

In vitro degradation of $Gd_2O_2S:Eu^{3+}_{5\%}$NPs

The potential toxicity of Gd complexes, already used for a long time as MRI contrast agents, is associated to their instability and ability to release trivalent Gd ions (Gd^{3+}). Consequently, before doing expensive and complex *in vivo* toxicity tests, we have first performed an *in vitro* biodegradation assay to evaluate the over-time stability of the product in different aqueous media: i) ultrapure water as a reference, ii) human plasma to gauge the potential degradation in the blood stream and iii) acidified buffer (pH=4.5) that mimics cell lysosomes. The NPs have been suspended in these media and kept at 37°C with regular sampling to test for the presence of degradation products in the supernatant (see Fig.2). After 6 months, the measured solubility of $Gd_2O_2S:Eu^{3+}_{5\%}$ NPs, both in water and human plasma was around 279 µM of Gd (equivalent to 43.9mg/L of Gd) in pure water and 82 µM (12.9mg/L of Gd) in human plasma. In comparison, the solubility of silica (SiO_2) is around 120 mg/L in water [39]. The lower solubility in human plasma could be due to several factors: higher pH (≈ 8 instead ≈6), human plasma is very rich in proteins (like albumin) which are known to form a corona around the NPs, stabilizing them and protecting them from degradation [40]; human plasma may contain anions, as phosphate for which Gd has a high affinity [41], which may form a very insoluble protective layer at the NPs surface. The dissolution phenomenon is very slow because even after 6 months the solution is not yet saturated.

It appears that $Gd_2O_2S:Ln^{3+}$ NPs are thermodynamically and kinetically very stable in these two media and will not release appreciable amount of Gd^{3+}. Thus, the dissolution of this product, even in a constantly renewed aqueous medium, should take years and years. This is very comforting when considering an introduction into the body by IV injection to use as contrast agent. The release of Gd ions from the NPs is therefore limited in this situation, which prevents the potential toxicity that has been described for some commercial linear gadolinium chelates contrast agents [42,43]. Indeed, after 14 days of incubation in human plasma, 27 µM of ionic Gd have been measured which corresponds to a dissolution of 0.05% of the NPs. A similar experiment [44] has demonstrated that commercial linear gadolinium chelates contrast agents presented a percentage of Gd leaching ranging from 1.1 to 21% after 15 days. This highlights the significant stability of the mineral NPs.

However, one must consider the fate of the NPs once they are done circulating in the bloodstream. It is well known that NPs are often taken up by the mononuclear phagocytic system. Once internalized, the preferred site of storage and degradation is the lysosome [45]. This cell compartment is much more acidic (pH = 4.5-5) and therefore more suited for NP solubilization.

Unsurprisingly, gadolinium release in the acidic medium (Fig.2) is drastically increased in comparison with water and plasma (100x and 300x higher, respectively). The mineral NPs are therefore susceptible to acidic degradation. However, even in this acidic condition, Gd_2O_2S NPs dissolution rate is very slow. After 30 days, the Gd^{3+} content in solution is equal 7.4 mM (equivalent to 1.4 g/L of NPs) from a suspension containing initially 20mg of NPs in 2mL (10 g/L). Therefore, only 14% of NPs have been dissolved. This value reaches 30% after 90 days. Maintaining the NPs in this medium will eventually dissolve the entirety of the NPs but at least for up to three months, the potential contrast variation induced by the remaining NPs will surely be sufficient for long term imaging and/or tracking.

In vivo monitoring of biodistribution, elimination and potential side-effects

Thereafter, we present two independent experiments designed to evaluate the distribution and potential side-effects of the NPs where rats received a single IV injection of pegylated NPs and were monitored over several months. The first one (#1) was conducted over 140 days using $Gd_2O_2S:Yb^{3+}{}_{4\%}/Tm^{3+}{}_{0.1\%}$ NPs for precise tracking inside the whole body thanks to their NIR imaging properties. The injected dose was purposefully low in order to test the sensitivity of our custom-made imaging system. The second one (#2) was conducted over 181 days using $Gd_2O_2S:Eu^{3+}{}_{5\%}$ NPs. The NPs injected dose was chosen higher than for the first study in order to get more pertinent information about eventual toxicity. Just like in the *in vitro* degradation experiment, the results (*in vivo* behavior) obtained here are expected to be analogous independently of the dopant that is being used (Eu^{3+} or Yb^{3+}/Tm^{3+}) considering the high similarity between the two NPs.

Live NIR imaging of$Gd_2O_2S:Yb^{3+}{}_{4\%}/Tm^{3+}{}_{0.1\%}$

During the injection, the fluorescence signal has been acquired downstream of the injection point (over the thorax area) every minute for 15 min as presented in Fig.3. The quantification of the signal/noise shows a good distribution in the blood pool: the signal increases progressively during the injection (first 7 min) and then decreases rapidly once the administration is complete, to finally disappear of the thoracic area after 11 min (See Fig.S3 for live animation). This indicates a good repartition of the NPs in the whole body and/or a rapid uptake by the macrophage-rich organs [45]. The signal measured in control animals does not fluctuate during the injection, reflecting the specificity of the detection.

Unlike MRI or CT, our custom-made imaging system does not enable full body scans, which necessitates the acquisition of several pictures. However, the higher sensitivity of this technique allows for the quantification of weaker signals. The signal distribution in the body was therefore methodically monitored through different acquisitions over different anatomical locations (thorax, liver, spleen, abdomen and bladder), showcasing the distribution in key organs generally involved in the metabolism

of NPs (lungs, liver, spleen, digestive tract and bladder) as can be seen in Fig.4.The fluorescence signal increases gradually over the liver area to reach a peak 14 days after injection. It then progressively decreases until almost complete disappearance after 140 days (in average, 80% of the signal is lost between days 14 and 140; Fig.4B). A similar profile was observed over the spleen (data not shown). This correlates with our previous tracking results obtained by MRI with $Gd_2O_2S:Eu^{3+}_{5\%}$ NPs [20]. The results also show a weaker signal over the thorax area that seems to disappear after 84 days. Like liver and spleen, the lungs act as a filter and are heavily irrigated organs. They are also a natural barrier against exterior aggressions and are therefore rich in resident macrophages probably responsible for NPs capture and degradation [46]. On the other hand, the signal collected over the abdomen and bladder doesn't vary significantly over-time (Fig.S4) indicating that these organs are not involved in the NPs capture process. Moreover, signal acquisition attempts on urine and feces were always negative, which indicates that the NPs are not directly excreted through urine or feces. The weak signal observed over the bladder at day 14 (Fig.4A) is probably due to an external contamination during the grooming of this particular animal given that no fluorescence signal was ever found in the urines.

At day 140, the organs were collected and signal acquisition was performed directly onto them to verify the results obtained on live animals. An intense signal was observed on the liver and spleen and a more discrete signal was found on lungs (Fig.5). This validates the hypothesis of NPs sequestration in those organs. It is important to consider here that the restricted signal localization appearing on those organs (Fig.5A) is only due to the limited laser illumination area. Indeed, sequential acquisitions revealed a homogenous repartition over their entire surface.

This means that there is a signal intensity differential between what is being detected on the surface of the skin and directly onto the actual target. This is the result of photon diffusion in the tissues as well as their limited penetrative power even though the wavelengths are optimized to be in the transparency window. Nevertheless, once again, this technique allows for unprecedented sensitive tracking of NPs.

The signal collected on the other major organs (heart, brain and kidneys) was not significantly different between tested and control animals attesting that they are not (or very weakly) involved in NPs metabolization (Fig.5B).

Quantification of $Gd_2O_2S:Yb^{3+}_{4\%}/Tm^{3+}_{0.1\%}$ and $Gd_2O_2S:Eu^{3+}_{5\%}$ distribution and excretion.

The organs were then prepared for ICP-MS analysis in both experiments to determine the Gd content and correlate with imaging results. As the fluorescence acquisitions demonstrated a homogenous repartition of the NPs in the organs, the results are here expressed in total quantity of Gd per organ obtained by reporting the measured concentration to the total organ mass (see Fig.S5 for original data). As presented in Table 1, in both experiments, the majority of the Gd was found in the liver and spleen.

Respectively, 163 µg and 46 µg where detected in the first experiment, corresponding to 35% and 10% of the initial $Gd_2O_2S:Yb^{3+}/Tm^{3+}$ load 140 days after IV injection. In the second experiment, 308 µg and 144 µg where detected, which corresponds to 11 and 5% of the initial $Gd_2O_2S:Eu^{3+}$ load 181 days after IV injection. It is interesting to note that in both experiments, the Gd concentration in spleen was much higher than in the liver (see Fig.S5) but the latter being much more massive, it accumulates a larger amount. A lower quantity was found in lungs (#1: 11 µg / 2% and #2: 43 µg / 1.5%). The traces of Gd found in brain, heart and kidneys where always non-detectable or non-significant, highlighting a potential specificity of the NPs towards macrophage-rich organs. Therefore, the organ distribution results established by mass spectrometry and by luminescence are congruent with one another.

The Gd content of the collected blood, urine and feces was also determined by ICP-MS to better understand the NPs dynamics and excretion mechanisms (Fig.6). In the first experiment (#1), the blood was not drawn directly after IV injections due to the simultaneous signal acquisition (see above). In consequence, the main peak does not appear. Two days after injection, a Gd circulating concentration of 160 µg/L remains in the blood compartment (Fig.6A). Subsequently, there is a rapid decrease in the circulating concentration until stabilization around 10 µg/L after four days which corresponds to the control level (animal injected with buffer solution without Gd NPs). In the second experiment (#2), a similar behavior is observed with a peak immediately after injection at 450 µg/L and subsequent decrease after five days at 0.5 µg/L. This kinetics corroborates the involvement of macrophage-rich organs in the rapid capture of NPs. After five days, the Gd concentration is very weak (<10µg/L) and in the same order of magnitude as control animals. It is at least 200 times below the LD_{50} given for Gd^{3+} ions [47]. According to Spencer *et al* [48], Gd salts have minimal toxicity under 10 mg/kg.

Only very small amounts of Gd were measured in urine (Fig.6B) with a maximum of 35 µg/L (#1) and 24 µg/L (#2). Urinary excretion of $Gd_2O_2S:Ln^{3+}$ NPs through kidneys can be considered as totally marginal and probably comes from rapid glomerular filtration of ionic Gd^{3+} ions traces present in blood. Indeed, the renal filtration cut-off threshold for NPs described in the literature is 8 nm [49–51] which is significantly lower than the diameter of the $Gd_2O_2S:Ln^{3+}$ NPs (ø = 130 nm).

On the other hand, we detected significant amounts of Gd in feces (Fig.6C): for #1, 113 ng/g on the second day progressively increasing until the first month to reach a maximum of 800 ng/g, then a pseudo-stabilization until the third month before returning to an excretion of about 80 ng/g in the fourth and fifth months. It should be noted that Gd traces where found in the feces of control animals, probably coming from exterior contamination since 26.7 ng/g and 9.8 ng/g have been found in food and litter, respectively, explaining the fluctuations observed in the measurements. For experiment #2, 100 ng/g where found on the first day with a consecutive peak after five days at 1750 ng/g and a slow decrease

from the first month to end up at 110 ng/g after 181 days. The NPs products of degradation therefore seem to be eliminated in the feces through the hepatobiliary system which is a known drainage route for particles of this size [47,54].

Whole body elimination rate

To gauge the total amount of Gd eliminated by natural ways at the experiments end points, the raw results found in urine and feces were normalized. The daily urine and feces output were considered to be respectively of 5.5mL/100g of body weight and 5g/day in average based on literature data [52] and extrapolations from samplings during isolation periods. From this, the AUC where calculated (see Fig.S6), leading to the conclusion that 2% (10 µg) and 69% (322 µg) of the initial $Gd_2O_2S:Yb^{3+}/Tm^{3+}$ load were eliminated respectively through urine and feces after 140 days in experiment 1. In experiment 2, those values fall to 0.5% (15 µg) and 11% (303 µg) of the initial $Gd_2O_2S:Eu^{3+}$ load after 181 days. Finally, adding those values to the total Gd amount found in isolated organs, the following amounts were recovered at the end of both experiments:

- experiment #1: 119% (48% organs, 2% urine, 69% feces)
- experiment #2: 29.5% (18% organs, 0.5% urine, 11% feces)

Therefore, it seems that the entirety of the initially injected Gd amount is recovered in #1. In #2, the cumulative amount only adds up to 29.5%. However, this last estimation is probably strongly underestimated due to the very low sampling days between day 1 and day 30, leading to the lack of detection of the maximum excretion peak in feces. In any case, the gap between Gd measurements and the expected values may also be explained by the discontinuous bile discharge during the day leading to the under-evaluation of the hepatobiliary elimination. All things considered and despite the fluctuations obtained in the Gd analysis, the results are coherent and seem to validate the hypothesis of a slow hepatobiliary degradation associated with a fecal excretion as well as a minor fixation in the lungs.

Examination of fixation in secondary tissues

For a more comprehensive and global view of the NPs distribution after IV injection, complementary analyses have been performed in the second experiment. Indeed, it is well known that the use of Gd-based contrast agents can lead to the fixation of Gd in bones and skin. Hydroxyapatites minerals composing bones have a high affinity for Gd ions [53] and the marrow contains resident macrophages susceptible to capture the NPs as demonstrated in the liver, spleen and lungs [54]. Furthermore, traces of Gd have been found in the skin of patients that received injections of such contrast agents, which could lead to fibrosis and other deleterious side-effects [55].

These two tissues have therefore been tested. No Gd was found in either of the skin samples (ears and skin from back and thorax) but traces of it were found in the bones. Analyses were conducted on whole

bone, diaphysis (mineral part), medullary cell compartment and medullary extracellular compartment (marrow supernatant) separately (see visual protocol in Fig.S7).The Gd concentration was similar in long bones (femur and humerus; around 8.7µg/g) and slightly lower in short bones (vertebrae and ribs; around 6.5µg/g). Regarding the sub-localization of the Gd, it appeared to be rather constant in the mineral part in both femur and humerus and respectively 2.5 and 4 times more concentrated in the marrow. Results clearly show that medullary extracellular compartment contain no Gd, meaning that Gd contained in the marrow is not in an ionic soluble form, otherwise it would probably have quickly diffused in the supernatant.

In order to better evaluate the total Gd content in bones, the skeleton has been estimated to 5% of the total body weight [56] and the concentration was averaged from the three tested bones giving a theoretical value of 132.5µg of Gd (5.3% of the initial load) fixed inside it after 181 days. Additionally, because we have demonstrated that the NPs are primarily eliminated through feces, the small intestine was also tested for traces of Gd that could have leaked out of the fecal matter and fixate in the surrounding tissue but no significant amount was found. Ultimately, an entire rat carcass (with organs already collected) was grinded and analyzed. The results show a Gd total amount of 118 µg (4% of initial load) which is comparable to the extrapolation above. This means that the remaining Gd in the body, appart from the liver, spleen and lungs, seems to be restrained in the skeleton (detailed results for Gd concentrations in organs can be found in Fig.S5).

Systemic toxicity evaluation

For both experiments, no differences in clinical state were ever observed between treated and control animals. Macroscopically, no signs of pain or weight loss were noticed: the body weights remained similar and within normal theoretical growth curves and the weights of the collected organs (liver, spleen, lungs, heart, brain, and kidneys) were comparable. The general observation did not reveal any trace of damage or apparent necrosis. After anatomo-pathological examination, the microscopic analysis of the histological slices from the first experiment did not reveal any tissue lesions (necrosis, edema, fibrosis, inflammation or lymphocytic cell infiltration) in the organs (See Table S1).

Additionally, we have commissioned a contract research organization (Jai Research Foundation) to perform a complementary acute toxicity study of $Gd_2O_2S:Eu^{3+}_{5\%}$NPs on Wistar rats to assess their safety.5 groups of 3 animals were intravenously injected with single shots of NPs (5% glucose water solution; 4 mL/Kg; injection time: 5 min) with increasing doses ranging from 13.2 to 400 mg/Kg. A following 14 days observation period did not reveal any mortality or signs of morbidity in any of the groups. No significant changes were observed in the body weight of individual animal and all showed normal food consumption throughout the study. Gross findings did not reveal any treatment related

toxicity in the animals (report available upon request).The sum of those results are consistent with our previous results [20] and unveils a relative innocuousness of $Gd_2O_2S:Ln^{3+}$ NPs.

Conclusions and Perspectives

Based on the results obtained in these studies, as well as the literature data [20,54,57], we propose the following scheme as an overview of the distribution, metabolism and excretion pathways of $Gd_2O_2S:Ln^{3+}$ NPs (see Fig.7). After injection into the blood compartment (I), the NPs circulate and are quickly captured by the highly vascularized organs rich in resident macrophages: mainly the liver and spleen and in a smaller proportion, the lungs and bone-marrow (II). A very small fraction of the Gd might leach from the NPs (III). Once captured, the NPs are degraded/metabolized most probably in the lysosomes of macrophages (IV) leading to the transformation of NPs (initially oxysulfides) into degradation by-products such as carbonates, phosphates or oxohydroxides that potentially lose their luminescence properties, before final excretion. This metabolism is slow and leads to the excretion mainly by feces (hepatobiliary system) and very weakly by urine (V).

The macrophage-rich organs where the NPs have been found to accumulate in this study have previously been described in the literature as targets for lanthanide based NPs like $NaLnF_4$ [57]. No significant Gd amounts have been detected in other vital organs, which decreases the concerns about potential off-target Gd fixation observed with some organic MRI contrast agents. The organ distribution is confirmed by NIR imaging up to a certain point. Indeed, the disappearance of the signal generated by the NPs seems to occur sooner than the actual clearance. This is most likely due to the fact that during the process of degradation, the NPs might not keep the structural conformation necessary for signal emission but are still detectable locally by mass spectrometry through their components. In any case, the NIR imaging system (NPs and custom-made imaging device) is very sensitive, even if it is perfectible. Indeed, we have been able to detect very low quantities of NPs in the body: for example in the thorax area 14 days after the injection. Under no circumstances would MRI or CT techniques allow such low detection threshold [20].

This degradation phenomenon is likely to happen in the lysosome of macrophages where the acidic conditions are favorable for degradation as demonstrated *in vitro*. We hypothesize that this process is slow enough that it doesn't impact their viability because the thorough examination of histological slices never revealed any trace of apoptosis or necrosis in isolated tissues.

Experiments show that the majority (>60%) of the injected product has been eliminated (primarily through feces) after 5 months. For the complete estimation of NPs metabolization/elimination kinetic, a

longer monitoring period, with more test animals and more regular sampling could be used to determine more precisely the total elimination duration and reduce the result dispersion (obtained with mass spectrometry). The analysis on fully homogenized samples collected over 24h would also be needed to take into account the discontinuous bile discharge during the day.

It is probable that full excretion of the remaining product will demand more than one year. This very long period of NPs retention in the body is unfortunately a serious drawback if one wants to consider a human application. The NPs diameter in this study (130 nm) was selected because it is the one that seemed better tolerated in our previous work where we tested them on mesenchymal stromal cells [20]. Such cells are more sensitive and fragile to external modifications (in this instance, the internalization of NPs) than macrophages. For clinical use, the design would surely need to be adapted and the overall diameter reduced for a faster elimination while maintaining good imaging performances. Very small NPs (< 8 nm) will be cleared from the body by renal filtration within hours of the injection [49,51], like commercially available contrast agents [58], but will not be suited for longitudinal studies and would probably suffer from poor performances. A diameter of 30 nm should therefore be a good compromise between a weaker retention time and acceptable associated toxicity. The drastic reduction of diameter should substantially change the *in vivo* behavior and dynamics of these NPs and will require an entirely new comprehensive study.

For a complete understanding of the *in vivo* behavior of these NPs, complementary experiments may be necessary. In particular, Gd traces have been found in small quantity in the bone tissue and in the marrow. This raises the question of potential long-term side-effects notably on hematopoiesis [54]. The *in vivo* transformation of oxysulfides into different by-products (like phosphates) also remains to be clarified. Indeed, lanthanide phosphates are probably the most insoluble mineral compounds that exist at neutral and basic pH and that they have been extensively studied for nuclear waste containment [59]. Hence, they are very effective to trap ionic Gd that could otherwise have toxic effects. Consequently, this slow transformation of oxysulfides into phosphate is not necessarily a crippling problem. Their formation would have a dual effect of preventing the release of toxic Gd ions but also increasing their retention time in the body. Unfortunately, the formed by-products are probably amorphous because we did not succeed in finding them after the *in vitro* degradation experiments, neither by X-ray diffraction nor by electron microscopy.

Even if clinical use is not yet an option (or at least in the near future), we believe that $Gd_2O_2S:Ln^{3+}$ NPs remain a very reliable tool for preclinical longitudinal explorations over a long period of time (several months). The results of this study show an excellent general tolerance, since no deleterious effects have been observed on animal health or isolated tissues. Moreover, no toxicity was reported after intravenous

bolus injection of up to 400 mg/kg. Consequently, this is paving the way for more global use in biomedical imaging.

Acknowledgements

We are grateful for Voxcan (Marcy l'Etoile, France) for their collaboration for distribution and excretion study on Wistar rats. We also warmly thank the Jai Research Foundation (Gujarat, India) for the acute toxicity study. This work was supported in part by CHROMALYS, INSERM and grants from the "RégionOccitanie" ("NANOTRACK" and "MULTIMAGE").

References

[1] H. Dong, S.-R. Du, X.-Y. Zheng, G.-M. Lyu, L.-D. Sun, L.-D. Li, P.-Z. Zhang, C. Zhang, C.-H. Yan, Lanthanide Nanoparticles: From Design toward Bioimaging and Therapy, Chem. Rev. 115 (2015) 10725–10815. https://doi.org/10.1021/acs.chemrev.5b00091.

[2] L.-D. Sun, Y.-F. Wang, C.-H. Yan, Paradigms and challenges for bioapplication of rare earth upconversion luminescent nanoparticles: small size and tunable emission/excitation spectra, Acc. Chem. Res. 47 (2014) 1001–1009. https://doi.org/10.1021/ar400218t.

[3] J. Shen, L.-D. Sun, C.-H. Yan, Luminescent rare earth nanomaterials for bioprobe applications, Dalton Trans. 0 (2008) 5687–5697. https://doi.org/10.1039/B805306E.

[4] R.B. Lauffer, Paramagnetic metal complexes as water proton relaxation agents for NMR imaging: theory and design, Chem. Rev. 87 (1987) 901–927. https://doi.org/10.1021/cr00081a003.

[5] W. Xu, K. Kattel, J.Y. Park, Y. Chang, T.J. Kim, G.H. Lee, Paramagnetic nanoparticle T1 and T2 MRI contrast agents, Phys. Chem. Chem. Phys. PCCP. 14 (2012) 12687–12700. https://doi.org/10.1039/c2cp41357d.

[6] M. Norek, E. Kampert, U. Zeitler, J.A. Peters, Tuning of the size of Dy2O3 nanoparticles for optimal performance as an MRI contrast agent, J. Am. Chem. Soc. 130 (2008) 5335–5340. https://doi.org/10.1021/ja711492y.

[7] H.M. Asl, Applications of Nanoparticles in Magnetic Resonance Imaging: A Comprehensive Review, Asian J. Pharm. AJP Free Full Text Artic. Asian J Pharm. 11 (2017). https://doi.org/10.22377/ajp.v11i01.1083.

[8] M.-A. Fortin, Nanoparticles for magnetic resonance imaging (MRI) applications in medicine, (n.d.). https://www.degruyter.com/view/NANO/nano.0053.00012 (accessed April 2, 2019).

[9] F. Carniato, K. Thangavel, L. Tei, M. Botta, Structure and dynamics of the hydration shells of citrate-coated GdF3 nanoparticles, J. Mater. Chem. B. 1 (2013) 2442–2446. https://doi.org/10.1039/C3TB20174K.

[10] Y. Tian, H.-Y. Yang, K. Li, X. Jin, Monodispersed ultrathin GdF3 nanowires: oriented attachment, luminescence, and relaxivity for MRI contrast agents, J. Mater. Chem. 22 (2012) 22510–22516. https://doi.org/10.1039/C2JM34987F.

[11] E.N.M. Cheung, R.D.A. Alvares, W. Oakden, R. Chaudhary, M.L. Hill, J. Pichaandi, G.C.H. Mo, C. Yip, P.M. Macdonald, G.J. Stanisz, F.C.J.M. van Veggel, R.S. Prosser, Polymer-Stabilized Lanthanide Fluoride Nanoparticle Aggregates as Contrast Agents for Magnetic Resonance Imaging and Computed Tomography, Chem. Mater. 22 (2010) 4728–4739. https://doi.org/10.1021/cm101036a.

[12] N.J.J. Johnson, W. Oakden, G.J. Stanisz, R. Scott Prosser, F.C.J.M. van Veggel, Size-Tunable, Ultrasmall NaGdF4 Nanoparticles: Insights into Their T1 MRI Contrast Enhancement, Chem. Mater. 23 (2011) 3714–3722. https://doi.org/10.1021/cm201297x.

[13] H. Xing, S. Zhang, W. Bu, X. Zheng, L. Wang, Q. Xiao, D. Ni, J. Zhang, L. Zhou, W. Peng, K. Zhao, Y. Hua, J. Shi, Ultrasmall NaGdF4 nanodots for efficient MR angiography and atherosclerotic plaque imaging, Adv. Mater. Deerfield Beach Fla. 26 (2014) 3867–3872. https://doi.org/10.1002/adma.201305222.

[14] T.J. Kim, K.S. Chae, Y. Chang, G.H. Lee, Gadolinium oxide nanoparticles as potential multimodal imaging and therapeutic agents, Curr. Top. Med. Chem. 13 (2013) 422–433.

[15] S.A. Osseni, S. Lechevallier, M. Verelst, C. Dujardin, J. Dexpert-Ghys, D. Neumeyer, M. Leclercq, H. Baaziz, D. Cussac, V. Santran, R. Mauricot, New nanoplatform based on Gd2O2S:Eu3+ core: synthesis, characterization and use for in vitro bio-labelling, J. Mater. Chem. 21 (2011) 18365–18372. https://doi.org/10.1039/c1jm13542b.

[16] S.A. Osseni, S. Lechevallier, M. Verelst, P. Perriat, J. Dexpert-Ghys, D. Neumeyer, R. Garcia, F. Mayer, K. Djanashvili, J.A. Peters, E. Magdeleine, H. Gros-Dagnac, P. Celsis, R. Mauricot, Gadolinium oxysulfide nanoparticles as multimodal imaging agents for T-2-weighted MR, X-ray

tomography and photoluminescence, Nanoscale. 6 (2014) 555–564. https://doi.org/10.1039/c3nr03982j.
[17] G. Ajithkumar, B. Yoo, D.E. Goral, P.J. Hornsby, A.-L. Lin, U. Ladiwala, V.P. Dravid, D.K. Sardar, Multimodal bioimaging using a rare earth doped Gd2O2S:Yb/Er phosphor with upconversion luminescence and magnetic resonance properties, J. Mater. Chem. B. 1 (2013) 1561–1572. https://doi.org/10.1039/c3tb00551h.
[18] S.-L. Lin, T.-Y. Liu, C.-L. Lo, B.-S. Wang, Y.-J. Lee, K.-Y. Lin, C.A. Chang, Synthesis, surface modification, and photophysical studies of Ln2O2S:Ln′3+ (Ln=Gd, Tb, Eu; Ln′=Tb and/ or Eu) nanoparticles for luminescence bioimaging, J. Lumin. 175 (2016) 165–175. https://doi.org/10.1016/j.jlumin.2016.01.037.
[19] L. Hernandez-Adame, N. Cortez-Espinosa, D.P. Portales-Pérez, C. Castillo, W. Zhao, Z.N. Juarez, L.R. Hernandez, H. Bach, G. Palestino, Toxicity evaluation of high-fluorescent rare-earth metal nanoparticles for bioimaging applications, J. Biomed. Mater. Res. B Appl. Biomater. 105 (2017) 605–615. https://doi.org/10.1002/jbm.b.33577.
[20] J. Santelli, S. Lechevallier, H. Baaziz, M. Vincent, C. Martinez, R. Mauricot, A. Parini, M. Verelst, D. Cussac, Multimodal gadolinium oxysulfide nanoparticles: a versatile contrast agent for mesenchymal stem cell labeling, Nanoscale. 10 (2018) 16775–16786. https://doi.org/10.1039/c8nr03263g.
[21] J. Santelli, C. Lepoix, S. Lechevallier, C. Martinez, D. Cussac, D. Calise, S. Moyano, M. Verelst, R. Mauricot, Up-conversion Gadolinium Oxysulfide Nanoparticles: Synthesis, Characterization and Use as Multimodal Probes for Bioimaging, Submiss. (n.d.).
[22] Y. Song, Y. Huang, L. Zhang, Y. Zheng, N. Guo, H. You, Gd2O2S:Yb,Er submicrospheres with multicolor upconversion fluorescence, RSC Adv. 2 (2012) 4777–4781. https://doi.org/10.1039/C2RA00009A.
[23] N. Wang, Z. Liu, H. Tong, X. Zhang, Z. Bai, Preparation of Gd2O2S: Yb3+, Er3+, Tm3+ sub-micro phosphors by sulfurization of the oxides derived from sol-gel method and the upconversion luminescence properties, Mater. Res. Express. 4 (2017) 076205. https://doi.org/10.1088/2053-1591/aa7e45.
[24] C.-H. Quek, K.W. Leong, Near-Infrared Fluorescent Nanoprobes for in Vivo Optical Imaging, Nanomaterials. 2 (2012) 92–112. https://doi.org/10.3390/nano2020092.
[25] G. Pratx, C.M. Carpenter, C. Sun, L. Xing, X-ray luminescence computed tomography via selective excitation: a feasibility study, IEEE Trans. Med. Imaging. 29 (2010) 1992–1999. https://doi.org/10.1109/TMI.2010.2055883.
[26] G. Pratx, C.M. Carpenter, C. Sun, R.P. Rao, L. Xing, Tomographic molecular imaging of x-ray-excitable nanoparticles, Opt. Lett. 35 (2010) 3345–3347. https://doi.org/10.1364/OL.35.003345.
[27] H. Chen, T. Moore, B. Qi, D.C. Colvin, E.K. Jelen, D.A. Hitchcock, J. He, O.T. Mefford, J.C. Gore, F. Alexis, J.N. Anker, Monitoring pH-triggered drug release from radioluminescent nanocapsules with X-ray excited optical luminescence, ACS Nano. 7 (2013) 1178–1187. https://doi.org/10.1021/nn304369m.
[28] H. Chen, F. Wang, T. Moore, B. Qi, D. Sulejmanovic, S.-J. Hwu, O.T. Mefford, F. Alexis, J.N. Anker, Bright X-ray and up-conversion nanophosphors annealed using encapsulated sintering agents for bioimaging applications, J. Mater. Chem. B. 5 (2017) 5412–5424. https://doi.org/10.1039/C7TB01289F.
[29] D. Avram, C. Tiseanu, Thermometry properties of Er, Yb-Gd2O2S microparticles: dependence on the excitation mode (cw versus pulsed excitation) and excitation wavelength (980 nm versus 1500 nm), Methods Appl. Fluoresc. 6 (2018) 025004. https://doi.org/10.1088/2050-6120/aa9ef9.
[30] European Medicines Agency, Gadolinium-containing contrast agents, (n.d.). http://www.ema.europa.eu/ema/index.jsp?curl=pages/medicines/human/referrals/Gadolinium-containing_contrast_agents/human_referral_prac_000056.jsp&mid=WC0b01ac05805c516f.

[31] Y. Forslin, S. Shams, F. Hashim, P. Aspelin, G. Bergendal, J. Martola, S. Fredrikson, M. Kristoffersen-Wiberg, T. Granberg, Retention of Gadolinium-Based Contrast Agents in Multiple Sclerosis: Retrospective Analysis of an 18-Year Longitudinal Study, AJNR Am. J. Neuroradiol. 38 (2017) 1311–1316. https://doi.org/10.3174/ajnr.A5211.
[32] A. Costa, A. Ronchi, P.D. Pigatto, G. Guzzi, Brain gadolinium deposition, hyperintense MRI signals, and resonance contrast agents, Magn. Reson. Imaging. 52 (2018) 137–138. https://doi.org/10.1016/j.mri.2018.06.001.
[33] H. Hifumi, S. Yamaoka, A. Tanimoto, D. Citterio, K. Suzuki, Gadolinium-Based Hybrid Nanoparticles as a Positive MR Contrast Agent, J. Am. Chem. Soc. 128 (2006) 15090–15091. https://doi.org/10.1021/ja066442d.
[34] T. Skotland, P.C. Sontum, I. Oulie, In vitro stability analyses as a model for metabolism of ferromagnetic particles (Clariscan((TM))), a contrast agent for magnetic resonance imaging, J. Pharm. Biomed. Anal. 28 (2002) 323–329. https://doi.org/10.1016/S0731-7085(01)00592-1.
[35] A. Tartaro, M.T. Maccarone, The utility of gadoteric acid in contrast-enhanced MRI: a review, Rep. Med. Imaging. (2015). https://doi.org/10.2147/RMI.S46798.
[36] J. Schindelin, I. Arganda-Carreras, E. Frise, V. Kaynig, M. Longair, T. Pietzsch, S. Preibisch, C. Rueden, S. Saalfeld, B. Schmid, J.-Y. Tinevez, D.J. White, V. Hartenstein, K. Eliceiri, P. Tomancak, A. Cardona, Fiji: an open-source platform for biological-image analysis, Nat. Methods. 9 (2012) 676–682. https://doi.org/10.1038/NMETH.2019.
[37] P. Thévenaz, M. Unser, User-friendly semiautomated assembly of accurate image mosaics in microscopy, Microsc. Res. Tech. 70 (2007) 135–146. https://doi.org/10.1002/jemt.20393.
[38] A. Vogel, V. Venugopalan, Mechanisms of Pulsed Laser Ablation of Biological Tissues, Chem. Rev. 103 (2003) 577–644. https://doi.org/10.1021/cr010379n.
[39] G.B. Alexander, W.M. Heston, R.K. Iler, The Solubility of Amorphous Silica in Water, J. Phys. Chem. 58 (1954) 453–455. https://doi.org/10.1021/j150516a002.
[40] G. Stepien, M. Moros, M. Pérez-Hernández, M. Monge, L. Gutiérrez, R.M. Fratila, M. de las Heras, S. Menao Guillén, J.J. Puente Lanzarote, C. Solans, J. Pardo, J.M. de la Fuente, Effect of Surface Chemistry and Associated Protein Corona on the Long-Term Biodegradation of Iron Oxide Nanoparticles In Vivo, ACS Appl. Mater. Interfaces. 10 (2018) 4548–4560. https://doi.org/10.1021/acsami.7b18648.
[41] A.D. Sherry, P. Caravan, R.E. Lenkinski, A primer on gadolinium chemistry, J. Magn. Reson. Imaging JMRI. 30 (2009) 1240–1248. https://doi.org/10.1002/jmri.21966.
[42] S. Laurent, L. Vander Elst, C. Henoumont, R.N. Muller, How to measure the transmetallation of a gadolinium complex, Contrast Media Mol. Imaging. 5 (2010) 305–308. https://doi.org/10.1002/cmmi.388.
[43] W.P. Cacheris, S.C. Quay, S.M. Rocklage, The relationship between thermodynamics and the toxicity of gadolinium complexes, Magn. Reson. Imaging. 8 (1990) 467–481.
[44] T. Frenzel, P. Lengsfeld, H. Schirmer, J. Hütter, H.-J. Weinmann, Stability of gadolinium-based magnetic resonance imaging contrast agents in human serum at 37 degrees C, Invest. Radiol. 43 (2008) 817–828. https://doi.org/10.1097/RLI.0b013e3181852171.
[45] J. Bourquin, A. Milosevic, D. Hauser, R. Lehner, F. Blank, A. Petri-Fink, B. Rothen-Rutishauser, Biodistribution, Clearance, and Long-Term Fate of Clinically Relevant Nanomaterials, Adv. Mater. Deerfield Beach Fla. 30 (2018) e1704307. https://doi.org/10.1002/adma.201704307.
[46] A. Ruiz, Y. Hernández, C. Cabal, E. González, S. Veintemillas-Verdaguer, E. Martínez, M.P. Morales, Biodistribution and pharmacokinetics of uniform magnetite nanoparticles chemically modified with polyethylene glycol, Nanoscale. 5 (2013) 11400–11408. https://doi.org/10.1039/c3nr01412f.
[47] E.B. Harstad, C.D. Klaassen, Gadolinium chloride pretreatment prevents cadmium chloride-induced liver damage in both wild-type and MT-null mice, Toxicol. Appl. Pharmacol. 180 (2002) 178–185. https://doi.org/10.1006/taap.2002.9385.

[48] A.J. Spencer, S.A. Wilson, J. Batchelor, A. Reid, J. Rees, E. Harpur, Gadolinium chloride toxicity in the rat, Toxicol. Pathol. 25 (1997) 245–255. https://doi.org/10.1177/019262339702500301.
[49] M. Yu, J. Zheng, Clearance Pathways and Tumor Targeting of Imaging Nanoparticles, Acs Nano. 9 (2015) 6655–6674. https://doi.org/10.1021/acsnano.5b01320.
[50] M.J. Ernsting, M. Murakami, A. Roy, S.-D. Li, Factors controlling the pharmacokinetics, biodistribution and intratumoral penetration of nanoparticles, J. Controlled Release. 172 (2013) 782–794. https://doi.org/10.1016/j.jconrel.2013.09.013.
[51] M. Longmire, P.L. Choyke, H. Kobayashi, Clearance properties of nano-sized particles and molecules as imaging agents: considerations and caveats, Nanomed. 3 (2008) 703–717. https://doi.org/10.2217/17435889.3.5.703.
[52] G.M. Otto, C.L. Franklin, C.B. Clifford, Chapter 4 - Biology and Diseases of Rats, in: J.G. Fox, L.C. Anderson, G.M. Otto, K.R. Pritchett-Corning, M.T. Whary (Eds.), Lab. Anim. Med. Third Ed., Academic Press, Boston, 2015: pp. 151–207. https://doi.org/10.1016/B978-0-12-409527-4.00004-3.
[53] J. Chen, T.J. Algeo, L. Zhao, Z.-Q. Chen, L. Cao, L. Zhang, Y. Li, Diagenetic uptake of rare earth elements by bioapatite, with an example from Lower Triassic conodonts of South China, Earth-Sci. Rev. 149 (2015) 181–202. https://doi.org/10.1016/j.earscirev.2015.01.013.
[54] T. Bose, D. Latawiec, P.P. Mondal, S. Mandal, Overview of nano-drugs characteristics for clinical application: the journey from the entry to the exit point, J. Nanoparticle Res. 16 (2014) 2527. https://doi.org/10.1007/s11051-014-2527-7.
[55] H. Yoldez, B. Ahlem, E. Abderrahim, Z. Faten, R. Soumaya, [Nephrogenic fibrosing dermatosis: From clinic to microscopy], Nephrol. Ther. 14 (2018) 47–49. https://doi.org/10.1016/j.nephro.2017.02.017.
[56] H.H. Donaldson, Quantitative studies on the growth of the skeleton of the albino rat, Am. J. Anat. 26 (1919) 236–314. https://doi.org/10.1002/aja.1000260204.
[57] Y. Sun, W. Feng, P. Yang, C. Huang, F. Li, The biosafety of lanthanide upconversion nanomaterials, Chem. Soc. Rev. 44 (2015) 1509–1525. https://doi.org/10.1039/c4cs00175c.
[58] A.N. Oksendal, P.A. Hals, Biodistribution and toxicity of MR imaging contrast media, J. Magn. Reson. Imaging JMRI. 3 (1993) 157–165.
[59] A. Shelyug, A. Mesbah, S. Szenknect, N. Clavier, N. Dacheux, A. Navrotsky, Thermodynamics and Stability of Rhabdophanes, Hydrated Rare Earth Phosphates REPO4 · n H2O, Front. Chem. 6 (2018) 604. https://doi.org/10.3389/fchem.2018.00604.

Figure Legends

Figure 1: Characterization of $Gd_2O_2S:Ln^{3+}$ nanoparticles after synthesis. A) Typical electron microscopy images (scale bar = 200 nm). B) X-ray diffractogram. Conventional room temperature emission spectra of C) $Gd_2O_2S:Eu^{3+}$ (under 365 nm excitation) and D) $Gd_2O_2S:Yb^{3+}/Tm^{3+}$ (under 980 nm excitation). Dotted lines delineate the wavelengths corresponding to each transitions.

Figure 2: Examination of *In vitro* leaching of gadolinium from $Gd_2O_2S:Eu^{3+}$NPs in different biological media. Gd concentration found in supernatant after long time incubation in water (µM, left axis), plasma (µM, left axis) and acidic medium mimicking lysosome (mM, right axis).

Figure 3: Distribution of the PEG-$Gd_2O_2S:Yb^{3+}/Tm^{3+}$ NPs during intravenous injection. A) Quantification of signal/noise ratio collected over the thorax area. B) Selection of corresponding images from 1 to 15min.

Figure 4: Evolution of fluorescence signal after intravenous injection of PEG-$Gd_2O_2S:Yb^{3+}/Tm^{3+}$ NPs. A) Scheme of the different illumination areas allowing the localization in target organs and reconstitution of the collected signal. B) Quantification of signal/noise ratio collected over liver and thorax (lungs) areas.

Figure 5: Anatomical distribution of PEG-$Gd_2O_2S:Yb^{3+}/Tm^{3+}$ NPs on isolated organs 140 days after intravenous injection. A) Collected fluorescence signal. B) Corresponding signal/noise quantification. Li: liver; S: spleen; Lu: lungs; H: heart; B: brain; RK: right kidney; LK: left kidney.

	#1Gd2O2S:Yb3+4%/Tm3+0.1% Day 140	#2Gd2O2S:Eu3+5% Day 181
Mean Gd injected (initial load = 100 %wt)	464 µg	2776 µg
Gd in organs (liver; spleen: lungs; heart; brain; kidneys)	224 µg (163; 46; 11; 3.5; 0; 0.1)	496 µg (308; 144; 43; 0.15; 0.04; 0.7)
	48 %wt (35; 10; 2; 0.75; 0; 0.02)	18 %wt (11; 5; 1.5; 0.005; 0.001; 0.02)

Table 1: Total amount of Gd in major organs (mean) determined by ICP-MS. Results presented as total quantity (µg) and percentage of initial load (%wt) at day 140 for the first experiment (#1, $Gd_2O_2S:Yb^{3+}{}_{4\%}/Tm^{3+}{}_{0.1\%}$) and day 181 for the second experiment (#2, $Gd_2O_2S:Eu^{3+}{}_{5\%}$).

Figure 6:Gd concentration in collected biological samples determined by ICP-MS: A) Blood; B) Urine and C) Feces.

Figure 7: Metabolism of $Gd_2O_2S:Ln^{3+}$NPs. I) Circulation of NPs after injection. II) Capture by abundantly irrigated, macrophage-rich organs. III) Potential Gd^{3+} leaching from NPs. IV) Degradation (most probably in the lysosomes of macrophages). V) Excretion of degradation products (or leached Gd^{3+}).

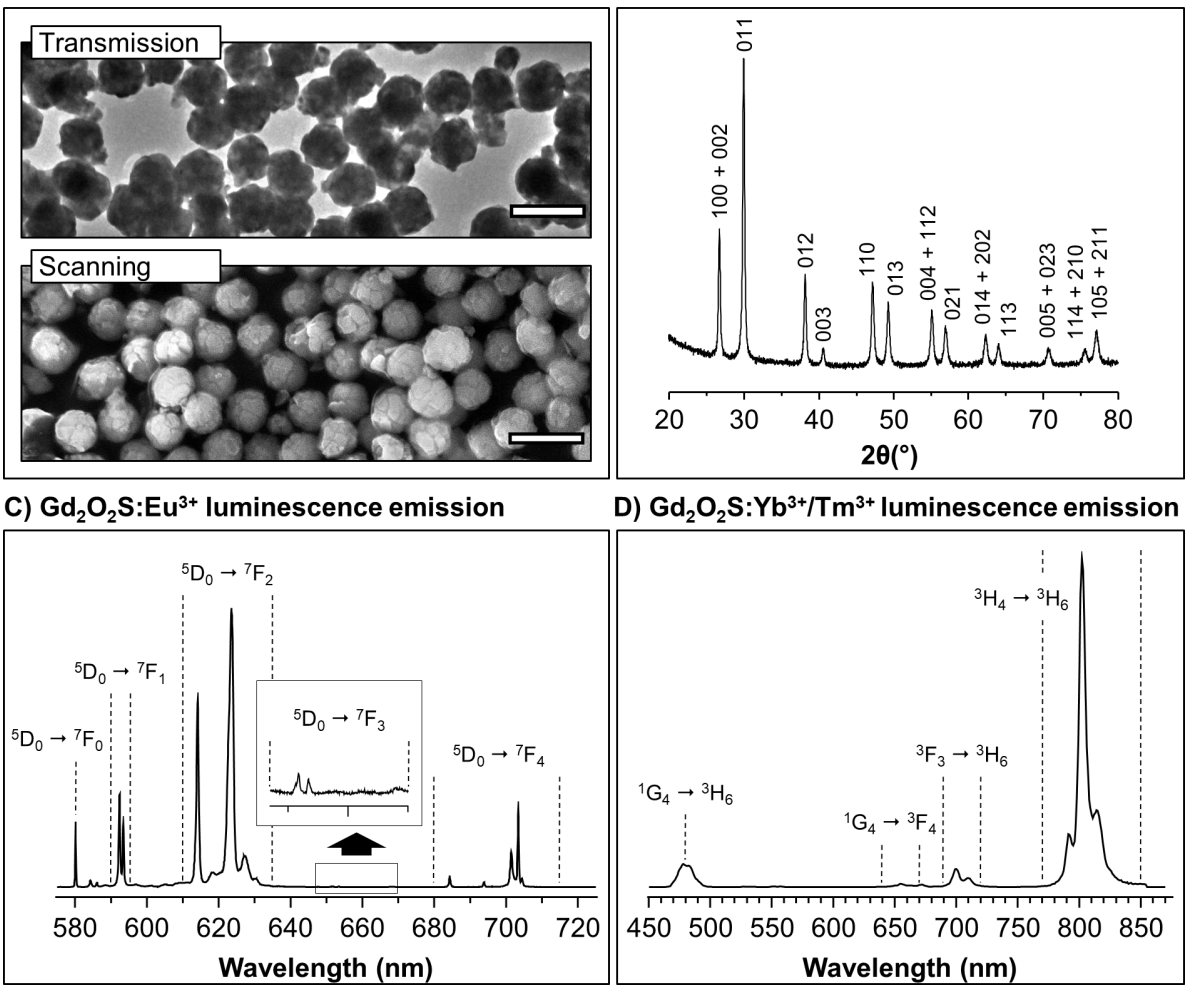
A) Electron Microscopy
Transmission
Scanning
B) X-Ray Diffraction
100 + 002
011
012
003
110
013
004 + 112
021
014 + 202
113
005 + 023
114 + 210
105 + 211
20
30
40
50
60
70
80
2θ(°)
C) Gd2O2S:Eu3+ luminescence emission
5D0 → 7F0
5D0 → 7F1
5D0 → 7F2
5D0 → 7F3
5D0 → 7F4
580
600
620
640
660
680
700
720
Wavelength (nm)
D) Gd2O2S:Yb3+/Tm3+ luminescence emission
1G4 → 3H6
1G4 → 3F4
3F3 → 3H6
3H4 → 3H6
450
500
550
600
650
700
750
800
850
Wavelength (nm)

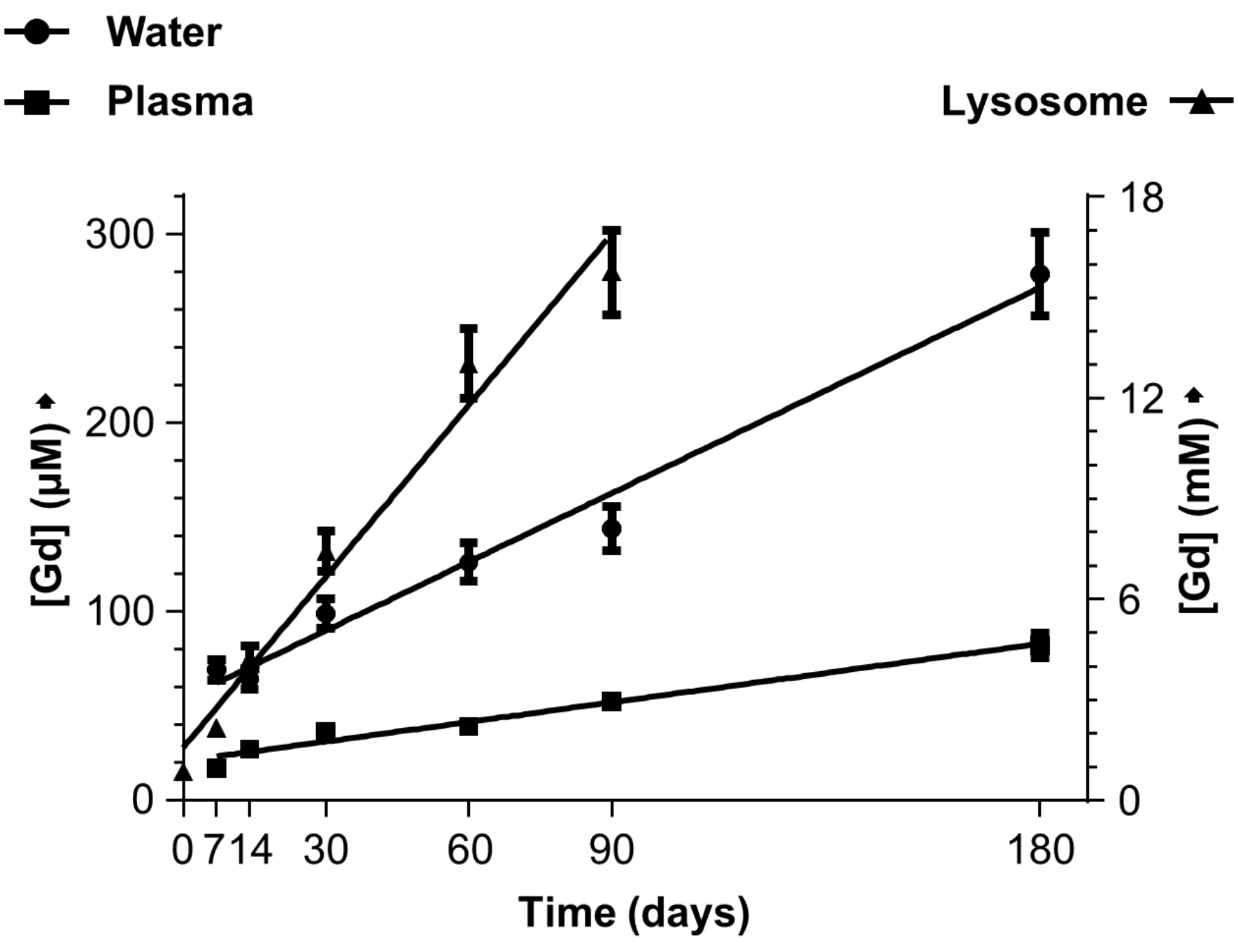
Water
Plasma
Lysosome
[Gd] (μM)
[Gd] (mM)
300
200
100
0
18
12
6
0
0 7 14 30 60 90 180
Time (days)

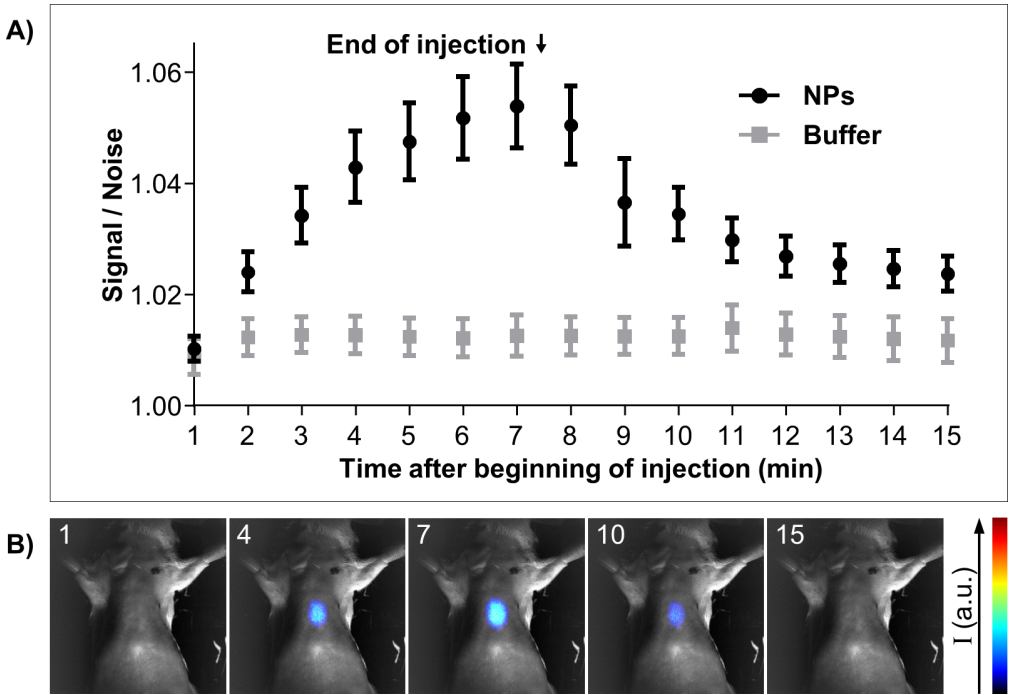
A)
End of injection
NPs
Buffer
Signal / Noise
1.06
1.04
1.02
1.00
1 2 3 4 5 6 7 8 9 10 11 12 13 14 15
Time after beginning of injection (min)
B)
1
4
7
10
15
I (a.u.)

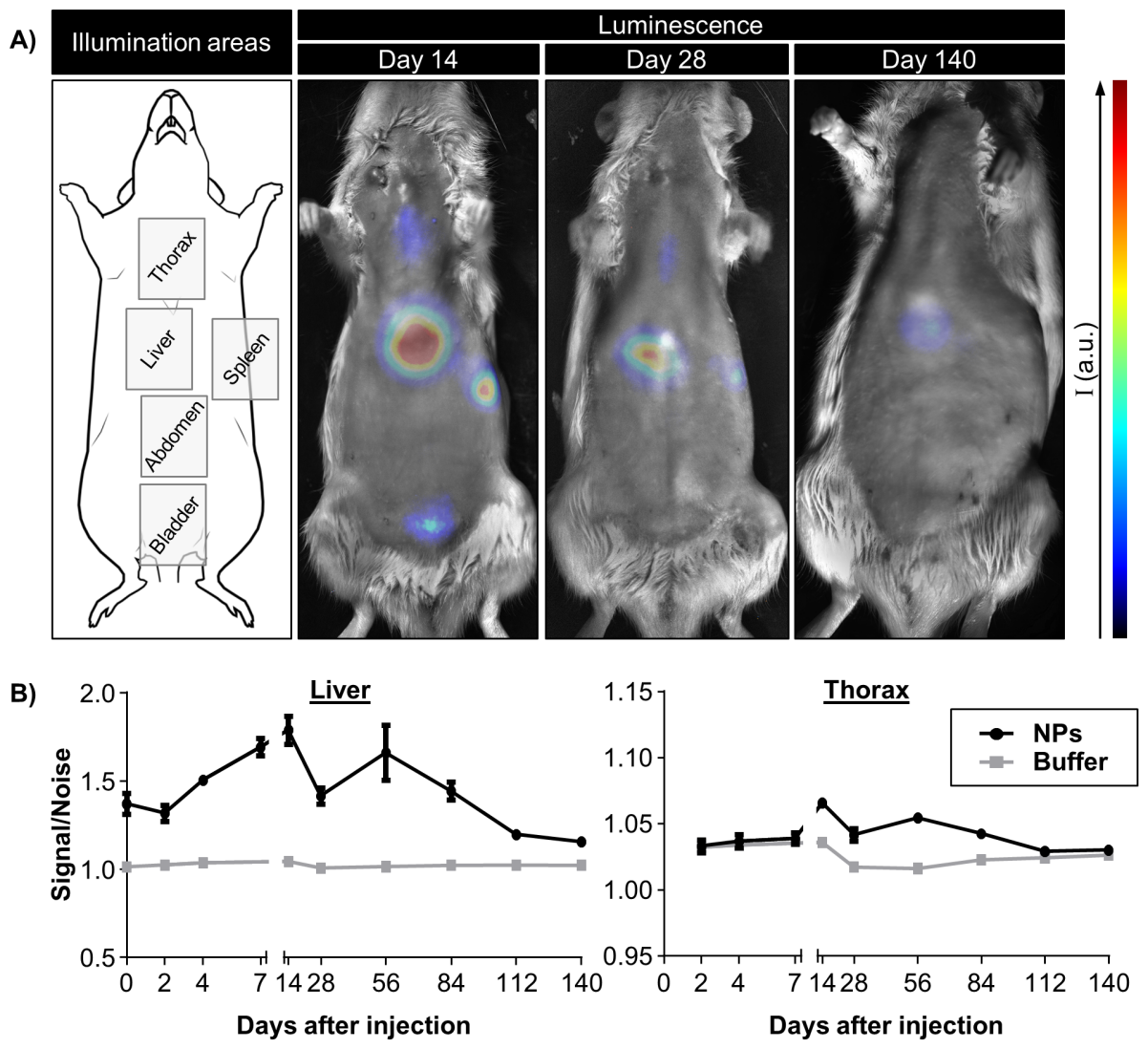
A)
Illumination areas
Luminescence
Day 14
Day 28
Day 140
Thorax
Liver
Spleen
Abdomen
Bladder
I (a.u.)
B)
Liver
Thorax
NPs
Buffer
Signal/Noise
2.0
1.5
1.0
0.5
1.15
1.10
1.05
1.00
0.95
0 2 4 7 14 28 56 84 112 140
Days after injection

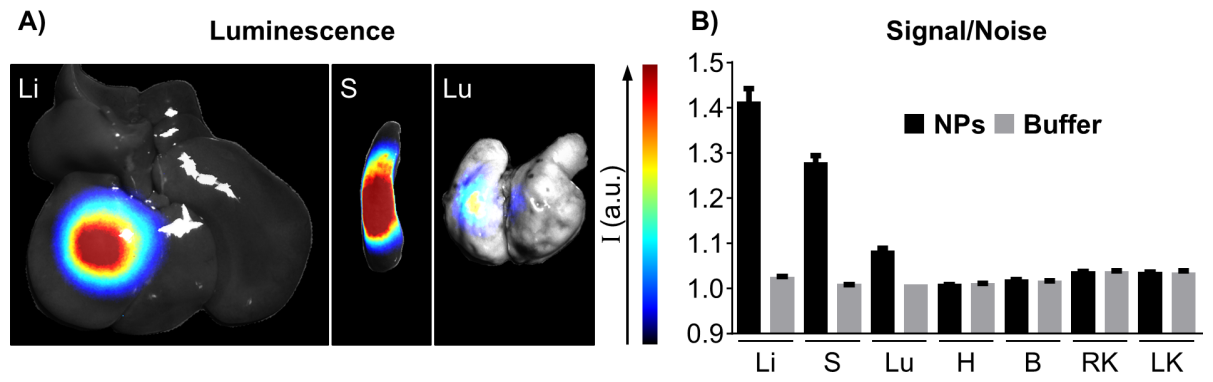
A)
Luminescence
Li
S
Lu
I (a.u.)
B)
Signal/Noise
NPs
Buffer
1.5
1.4
1.3
1.2
1.1
1.0
0.9
Li
S
Lu
H
B
RK
LK

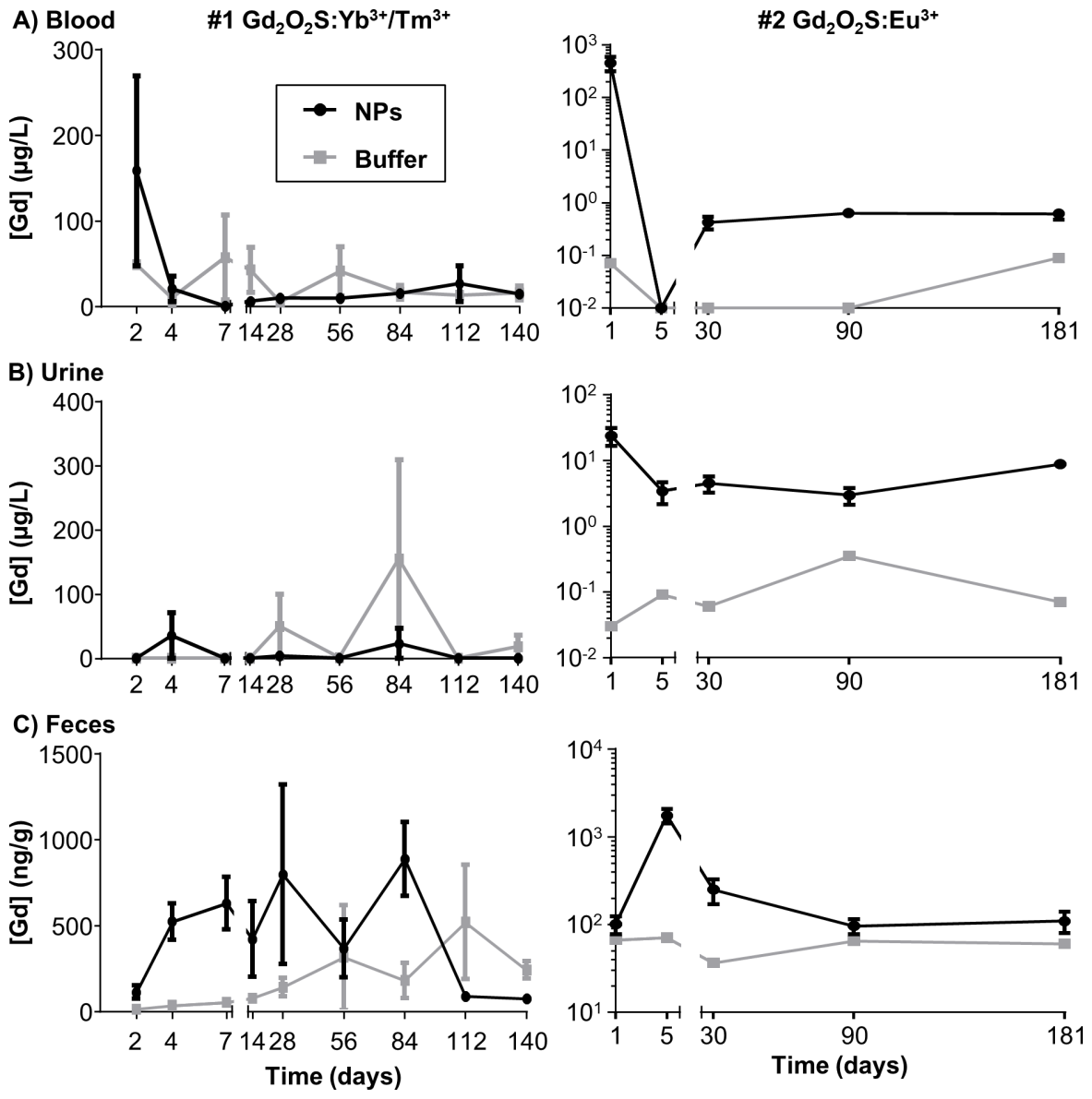
A) Blood
#1 $Gd_2O_2S:Yb^{3+}/Tm^{3+}$
#2 $Gd_2O_2S:Eu^{3+}$
NPs
Buffer
[Gd] (µg/L)
B) Urine
[Gd] (µg/L)
C) Feces
[Gd] (ng/g)
Time (days)
Time (days)

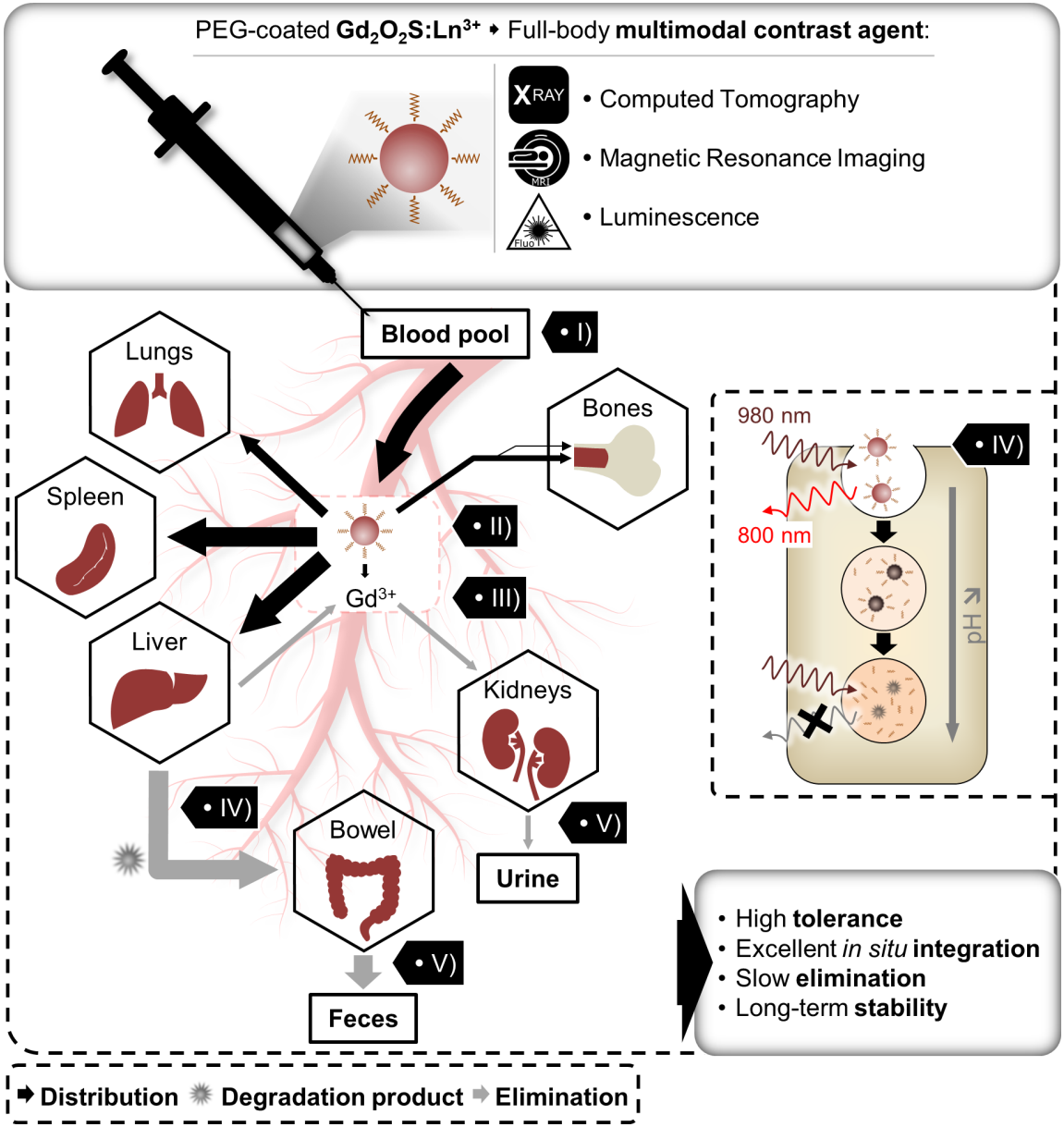
PEG-coated $Gd_2O_2S:Ln^{3+}$ ➧ Full-body **multimodal contrast agent**:
XRAY
• Computed Tomography
MRT
• Magnetic Resonance Imaging
Fluo
• Luminescence
Blood pool
• I)
Lungs
Bones
Spleen
• II)
Gd^{3+}
• III)
Liver
Kidneys
• IV)
Bowel
• V)
Urine
• V)
Feces
980 nm
800 nm
• IV)
pH
• High **tolerance**
• Excellent *in situ* **integration**
• Slow **elimination**
• Long-term **stability**
➧ **Distribution** ✹ **Degradation product** ➧ **Elimination**

$Gd_2O_2S:Ln^{3+}$ nanoparticles

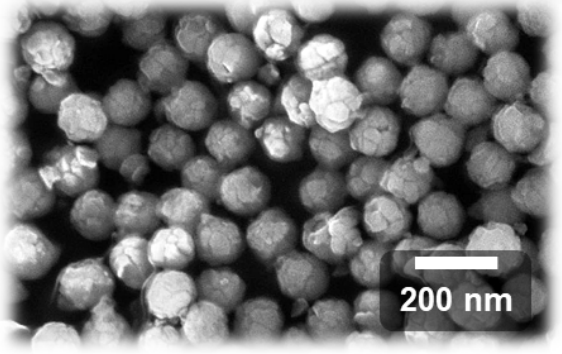

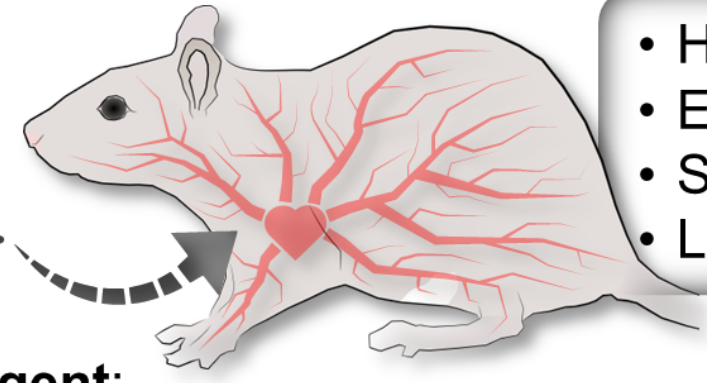

- High **tolerance**
- Excellent *in situ* **integration**
- Slow **elimination**
- Long-term **stability**

multimodal contrast agent:

Computed Tomography | Magnetic Resonance Imaging | Luminescence

- XRAY
- MRI
- Fluo